



Experimental investigation on anti-sliding performance of grouted micro-pipe pile groups

Xiaoli Liu^{1,2} · Yushuang Liu^{1,2} · Kai Liu² · Yuanyuan Su²

Received: 19 August 2021 / Accepted: 4 April 2022 / Published online: 16 April 2022
© The Author(s), under exclusive licence to Springer Nature B.V. 2022

Abstract

As a common geohazard, landslides may cause enormous losses of human lives and properties. It is necessary to prevent landslides by effective technical measures. The grouted micro-steel-pipe pile group is a typical composite anti-sliding structure applied in landslide-stabilization engineering, where the micropiles and the surrounding geomaterials interact to resist the landslide thrust. In this study, laboratory experiments were carried out to investigate the anti-sliding performance of a kind of 3×3 grouted micro-pipe pile group anchored in bedrock at different row spacing of micropiles. The results indicate that the grouted micro-pipe pile group shows a relatively large anti-sliding capacity at row spacing of 4–8 times the micropile diameter. The active earth pressure on micropiles induced by soil movement shows an approximately triangular distribution. More of the thrust load transfers from the rear pile row to the middle and front pile rows gradually as the thrust load increases, where the ratios of earth thrust among the rear, middle and front pile rows can reach up to 1:0.60:0.44. The maximum bending moment occurs at the anchoring segment close to the bedrock surface. As the thrust loading increases, the maximum bending moment of the rear pile row will first increase to a peak value and then rapidly decrease, implying the micropile group is about to lose its anti-sliding ability. The development of deformation can be characterized as three stages including the slow deformation stage, accelerating deformation stage and unstable deformation stage. It is recommended that the horizontal displacement of pile head should be less than 1% of the loading depth for actual engineering design.

Keywords Landslide stabilization · Grouted micro-pipe pile group · Row spacing · Anti-sliding capacity · Lateral thrust load

✉ Xiaoli Liu
LXL4791@ouc.edu.cn

¹ Shandong Provincial Key Laboratory of Marine Environment and Geological Engineering, Ocean University of China, Qingdao 266100, China

² College of Environmental Science and Engineering, Ocean University of China, Qingdao 266100, China

1 Introduction

Landslides are a ubiquitous hazard which threaten human lives and destroy infrastructures (Chandrasekaran et al. 2013; Zhang et al. 2021), particularly in mountainous areas. Due to the increase of extreme climates and the intensification of geological activities, the risk of landslide occurrence has remarkably increased worldwide. Furthermore, human-activity-induced landslide occurrence is increasing (Froude and Petley 2018). Therefore, how to reduce the disasters caused by landslides has always been a concern for geotechnical engineers. As an effective technical measure, different kinds of anti-sliding structures have been applied to reinforce the landslides or unstable slopes (Cantoni et al. 1989; Juran et al. 1996; Li et al. 2020; Liu et al. 2021; Kumar et al. 2021).

Micropiles are one of the anti-sliding structures that have been widely used in landslide-stabilization engineering (Cantoni et al. 1989; Juran et al. 1996; Loehr et al. 2000; Sun et al. 2013; Hu et al. 2016). Micropile, also known as mini-pile, is drilled and grouted pile in small diameter typically less than 300 mm and the slenderness ratio greater than 30 (Bruce and Juran 1997; Xiao et al. 2009). The reinforcement in a micropile may be a single or several reinforcing bars, a steel pipe, and a rolled structural steel (Sun et al. 2013). Due to the relatively low stiffness and bearing capacity of a single micropile, micropiles are often applied as a group configuration or a composite structure combined with other kinds of anti-sliding structures practical engineering (Bruce et al. 2005; Hu et al. 2016; Prat 2017; Kim et al. 2018).

Compared with the conventional large diameter anti-sliding piles, the main advantages of micropiles can be concluded as simple and fast installation, economic construction, and good site flexibility with minimal disturbing the slope stability, especially for landslides in mountain areas (Sun et al. 2013; Hu et al. 2016; Xiang et al. 2015; Yang et al. 2022). As indicated in Fig. 1, the grouted micro-steel-pipe pile group is a typical composite anti-sliding structure used for landslide stabilization in the last decade; the steel pipe in diameter of 100–200 mm is placed in the borehole as reinforcement, and the flowable grout is injected into the drilled hole under pressures of a certain value (Xiang et al. 2015). The grout is an important part of the micropile, which can enhance the shear strength of deposits close to the micropile by infiltrating into the surrounding ground under high-pressure injections; moreover, the grout can prevent the steel pipe from corrosion (Aboutabikh et al. 2020). In

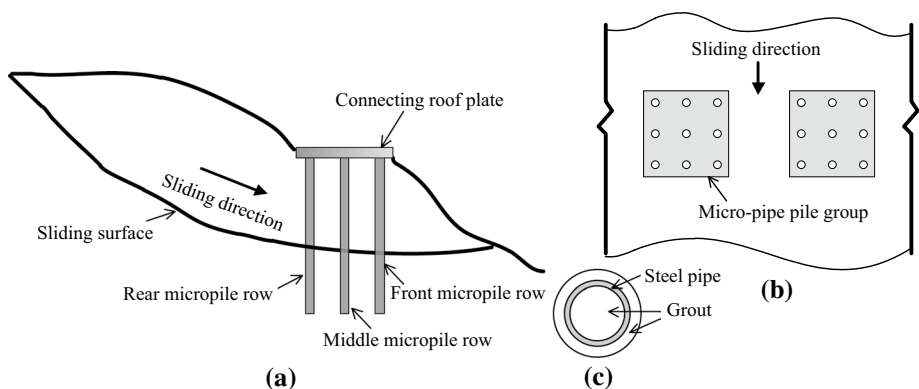


Fig. 1 Diagram of the grouted micro-pipe pile groups employed in slope stabilization. **a** Cross section of the pile-slope system, **b** Plane diagram of pile-slope system, **c** Cross section of the grouted micro-pipe pile

practice, some micro-pipe piles are usually connected into an integration by rigid beams or plates on top of the piles. Therefore, the micropiles, the connecting rigid beams or plates and the rock-soil mass surrounding micropiles constitute a composite anti-sliding structure to resist the sliding thrust load.

Although some investigations on the property of landslide-stabilization micropiles have been conducted by experiments, numerical simulations and theoretical analysis (Sun et al. 2013; Xiang et al. 2015; Zeng and Xiao 2019; Gupta and Chawla 2020; Li et al. 2020; Ghosh et al. 2021), most of the literature did not pay attention to the influence of row spacing of micropiles on anti-sliding capacity of the micropile group. Sun et al. (2013) suggested that the row spacing of micropiles in line should be greater than 7 times pile diameter to decrease the pile group effects in stabilization design of earth slopes, according to conclusions by Bruce et al. (2005) from investigations of micropiles in foundation engineering. However, the authors did not propose the maximum value of row spacing appropriate for stabilizing landslides. Zeng and Xiao (2019) computed the internal forces of the 3×3 micropile groups stabilizing earth slopes by a simplified analytical method; their results indicated the row spacing of micropiles in a micropile group had little influence on the internal forces. However, it is well known that ignoring the effect of row spacing is unreasonable for practical engineering design of stabilizing landslide by micropile groups. Li et al. (2020) experimentally investigated the mechanical characteristics of micropiles arranged in triple rows supporting soil landslide. The results indicated that the bending moments on different rows of micropiles were slightly different prior to failure of the soil slope. However, the bending moments on the rear and middle row piles are much larger than that on the front row piles due to failure of the soil slope. Unfortunately, the effect of row spacing on performance of micropiles was not taken into consideration in their experiments.

To date, there are still some aspects needing to be further explored on properties of micropile groups for stabilizing landslides, especially the influence of row spacing of micropiles on the anti-sliding performance of the micropile groups. In this study, laboratory experiments were conducted to improve the understanding of anti-sliding behavior of the grouted micro-pipe pile group in 3×3 configuration that was used to stabilize the landslide where the main slip surface was the overlying deposit-bedrock contact surface and the sliding mass moved mainly along the bedrock. Characteristics of this kind of composite anti-sliding structure, such as active earth pressure, bending moment, deformation process and the influence of row spacing on anti-sliding performance, were investigated, which can provide experimental data for engineering application.

2 Materials and method

2.1 Test setup

As shown in Fig. 2, based on the test setup used by White et al. (2008) to investigate the characterization of slender pile behavior subject to lateral soil movements, the experiment setup in this study is constituted by the shearing system, loading system and a data acquisition system. The shearing system includes an upper and a lower shear boxes and two sliding rails installed between the shear boxes. The lower shear box is fixed and connected with the reaction frame, while the upper shear box can horizontally move along the rails, which can induce lateral translation of soils to simulate the free-field movement of sliding

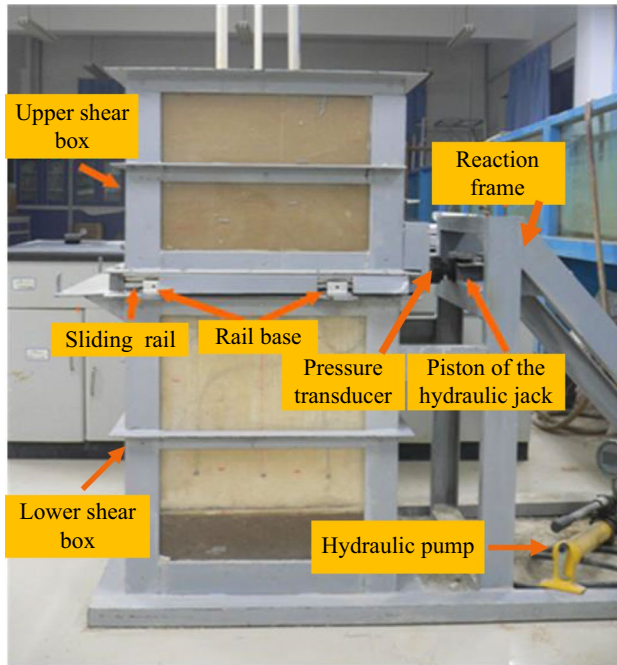


Fig. 2 Test setup

soil; in this way the lateral thrust load caused by soil movements can be applied to micro-pile groups.

The shear box is made of perspex in 8 mm thick, using the angle iron as the supporting frame. There is a 4 mm gap between the upper and lower shear boxes. Heights of the upper and lower shear boxes are 500 mm and 700 mm, respectively, and the internal width and length of the shear box are both 600 mm.

The loading system is constituted by a hydraulic jack, a pressure transducer, and the reaction frame. The pressure transducer is installed on the side of the upper shear box, about 55 mm above the lower shear box. The magnitude of applied lateral thrust load is controlled according to the readings of the pressure transducer.

A data acquisition system records the testing data, which is consist of data acquisition boxes, a power supply cell, and the corresponding software.

2.2 Materials

According to the dimensions of the micropiles commonly used in practical engineering, the geometric similarity scale between the prototype and the model in this study could be 10–18. In accordance with the similarity theory of geo-mechanical model test (Iai 1989) and the familiar physical and mechanical parameters of deposits and bedrock in landslide, materials for the experiments were selected to meet the requirements of similarity law of the main properties.

The sliding mass was made of sand and barite powder at the ratio of 7:1 with the water content of 5%; the sliding zone was made of talc powder and gypsum at the ratio

of 100:1 with the water content of 5%–6%; the bedrock was simulated by the mixture of barite powder, gypsum, sand, and water at the ratio of 12:1:10:2.5. The bedrock block in dimensions of 600 mm × 600 mm × 500 mm (i.e., length × width × height) was used in tests after natural dried for about 30 days. The averaged parameters of model materials including the bedrock, sliding mass and sliding zone are tabulated in Table 1.

In the experiments, the borehole diameter of the micropile was 16 mm, a polypropylene (PP) pipe was placed in the center of the borehole, and then the grout was injected into the borehole to form a grouted pipe pile after the grout solidification. The PP pipe was 12 mm in outer diameter, 2 mm in wall thickness and 800 mm in length with 500 mm above the bedrock surface and 300 mm embedded in the bedrock. Young's modulus of the PP pipe was 2.04 GPa, the Poisson's ratio was 0.4 and the yield tensile stress was about 16 MPa.

The grout was mixed at a talcum powder–cement–water ratio of 2:1:3. The physical and mechanical properties were tested after natural dried for about 4 days. The unit weight of the grout was 21 kN/m³, the Young's modulus was 200 MPa, the tensile strength was 0.15 MPa and the compressive strength was 1.8 MPa.

2.3 Experiment scheme

As shown in Fig. 3, each micro-pipe pile group consisted of nine micropiles arranged in 3 × 3 pattern forming a rectangular cross section. Besides, the micropiles were connected as an integration by a rigid roof plate on the top of piles. The lateral spacing of micropiles in row (i.e., the pile spacing) was $S = 3D$ (D is the diameter of the micropile), and the longitudinal spacing of micropiles in line (i.e., the row spacing) L_s was 2D, 4D, 6D and 8D, respectively. Two sets of the micropile group were constructed in each test with the center distance between them of 250 mm.

As presented in Fig. 3, the test micropiles in the experiments were labeled as 1, 2 and 3 respectively. The strain gauges were symmetrically adhered to both sides of each test micropile to obtain longitudinal strains of the pile; these strains will be used to calculate the bending moments of the micropile. At each location marked as a, b and c, four earth pressure cells numbered as E1, E2, E3 and E4 were installed to record the active earth pressures on micropiles. In total, there were nine couples of strain gauges and four earth pressure cells for each test pile along the buried depth, as shown in Fig. 3a.

In addition, displacement transducers were deployed on the rigid roof plate to measure the horizontal displacements of the pile head. The lateral thrust load was generated in stages with an increment of 0.5 kN by the hydraulic jack.

Table 1 The averaged parameter of model material

Material	Unit weight kN/m ³	Cohesion kPa	Internal friction angle degree	Young's modulus MPa	Compressive strength MPa	Tensile strength MPa
Sliding mass	18	6	35	N/A	N/A	N/A
Sliding zone	15	2	27	N/A	N/A	N/A
Bedrock	23	193	53	230	1.25	0.13

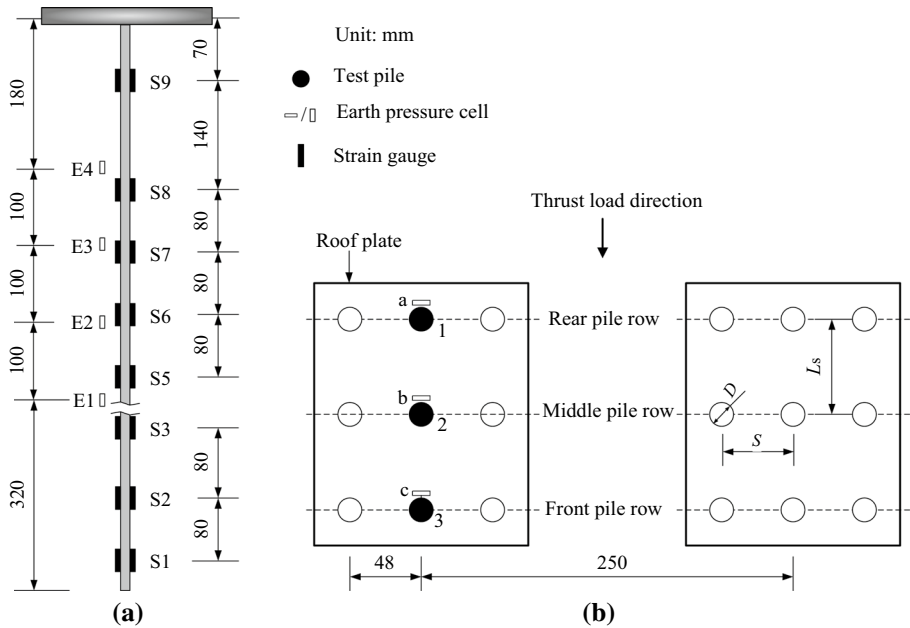


Fig. 3 Layout of the experiments. **a** Strain gauges and earth pressure cells along each test pile; **b** Arrangement of micropile groups on the plane

2.4 Experiment procedure

- (1) Model materials were prepared and the bedrock blocks were made first. PVC pipes in 16 mm diameter were used to reserve pile bores according to the test design, that is, PVC pipes in diameter of 16 mm were inserted into the bedrock before it gained the high strength to reserve the pile bores.
- (2) The model was constructed by filling the bedrock block, the sliding zone and sliding mass materials into the shear boxes in sequence, during which the earth pressure cells were installed.
- (3) The PVC pipes were pulled out to form the pile bores, and subsequently, PP pipes in 12 mm diameter were inserted into the pile bores, and then the grout was injected into the bores until all the bores were filled with grout.
- (4) The rigid roof plate on the top of micropiles was cast using cement mortar. The roof plate was in 30–40 mm thickness with a wire netting in it.
- (5) About four days later, the pressure transducer, strain gauges and earth pressure cells were linked with the data logger. Two displacement transducers were deployed to measure the horizontal displacements of the pile head. Subsequently, the lateral thrust load was applied on the upper shear box with a hydraulic jack; during this process the thrust load was increased at the increment of 0.5 kN. When the readings of test data under a certain load remained almost unchanged, the next stage of load was then applied. The test data were recorded in real-time until the micropile group lost its bearing capacity.

3 Results and discussion

3.1 Active earth pressure on micropiles

In this study, the part of the micropile above the bedrock surface subjected to the lateral thrust load is termed as the loading segment; while the part of the micropile embedded in bedrock is termed as anchoring segment.

As presented in Fig. 4, the active earth pressure (i.e., earth pressure on the upslope side of micropiles directly induced by soil movements) on each row of micropiles showed an approximately triangular distribution below a depth of 0.28 m from the pile head. There was little earth pressure on the segment of the pile between the depth of 0.28 m and the pile head, which indicated the pile-soil relative displacement of the corresponding segment of the pile was very small; this may response to the flexibility of the micropiles and the sliding pattern of the slope that the sliding mass moved mainly along the bedrock surface. As the depth increased, the active earth pressure increased gradually, indicating the increased relative displacement between micropiles and soils. The earth pressure reached the maximum at depth of 0.48 m close to the sliding surface. The active earth pressure on the micropiles increased nonlinearly with the increasing thrust load, i.e., the larger the thrust load was, the faster the active earth pressure increased.

Figure 5 shows the comparison of active earth pressures on micropiles of front row, middle row and rear row under different thrust loads, from which it can be observed that the active earth pressure on the rear pile row was notably larger than that on the other two rows, indicating that the rear row of micropiles endured more of the lateral thrust load induced by soil movements. The active earth pressures on the middle and front rows of piles were basically the same for thrust loads less than 5.0 kN. For the case of thrust load of 5.0 kN, the active earth pressure on the middle row became larger than that on the front row. As what will be discussed later on, the micropile group had experienced a relatively large deformation at the thrust load of 5.0 kN, approaching the critical state of failure.

For further analysis, the ratios of active earth pressures among different rows of micropiles at row spacing of 6D were calculated. When the thrust load was 3 kN, the active earth pressure ratios among the rear, middle and front rows of piles were 1:0.38:0.38; and the ratios were 1:0.51:0.49 and 1:0.60:0.44 for thrust loads of 4 kN and 5 kN, respectively. With the increasing thrust load, much more of the earth thrust

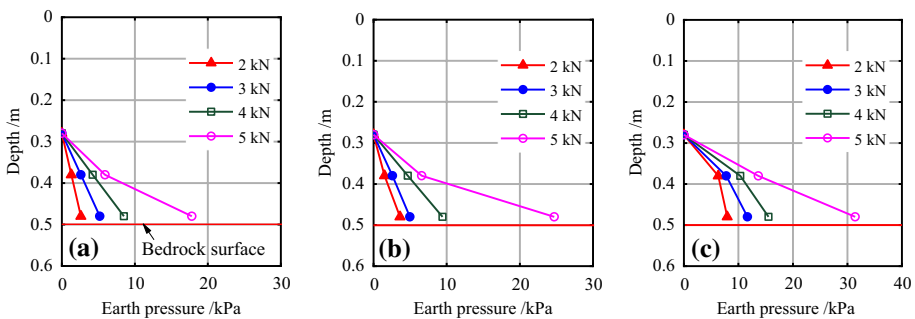


Fig. 4 Active earth pressure on micropiles at row spacing of 6D under various thrust load. **a** The front pile row; **b** The middle row; **c** The rear pile row

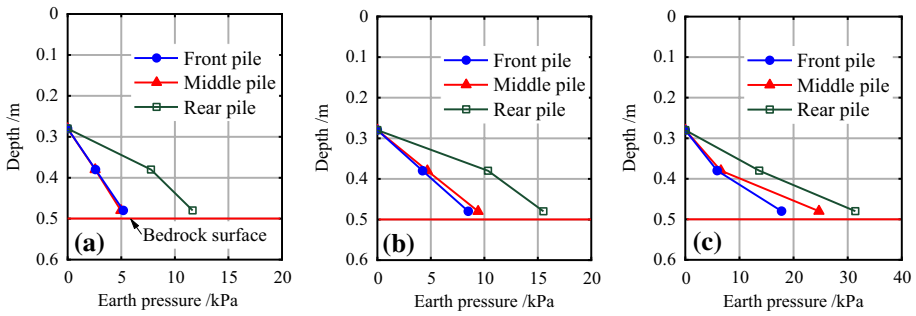


Fig. 5 Active earth pressure on micropiles at row spacing of 6D under the thrust loads of **a** 3.0 kN, **b** 4.0 kN and **c** 5.0 kN

transferred from the rear pile row to the middle and front pile rows, where the active earth pressure on the middle pile row increased much greater.

3.2 Deformation characteristics of the micropile group

3.2.1 Deformation pattern

Figure 6 shows the deformation pattern of micropile group in the tests, where Fig. 6a displays the deformation of loading segment with a relatively large flexural deformation within 20 cm above the bedrock surface; this caused crush of the grout layer of the micropile in the associated region. For the section of the micropile between 20 cm above the bedrock surface and the pile-head, the grout layer remained relatively intact due to the small flexural deformation. The deformation characteristics of the loading segment were consistent with the distribution feature of active earth pressure on piles.

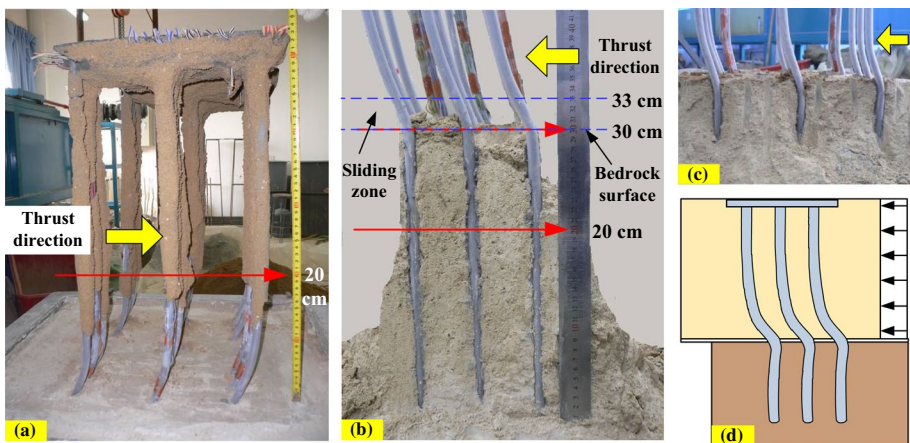


Fig. 6 Deformation of the 3×3 micropile group. **a** Deformation of micropiles above the bedrock surface, **b** Deformation of micropiles near and below the sliding surface; **c** Deformation of micropiles near the sliding zone; **d** Sketch of the deformation pattern of the micropile group

Fig. 7 Horizontal displacement of the micropile head

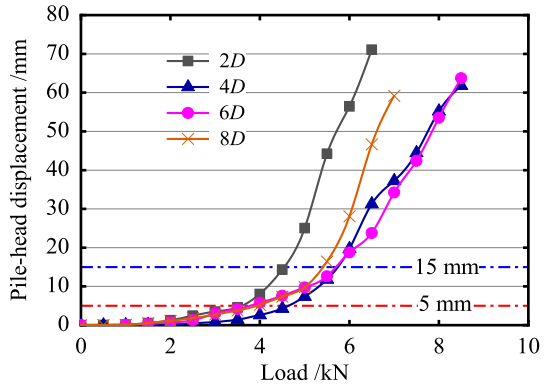
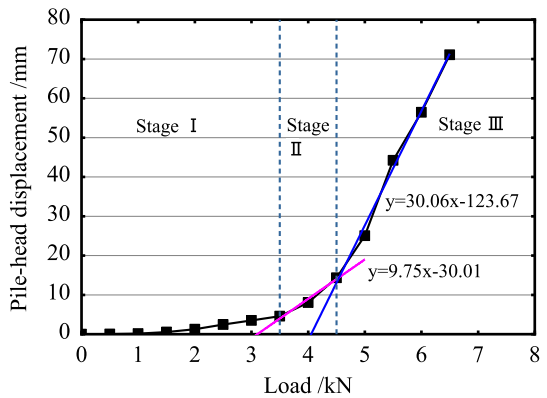


Fig. 8 Three stages of the micro-pile-group deformation (2D)



As indicated in Fig. 6b, c, the anchoring segment of micropiles was closely integrated with the bedrock. The flexural deformation concentrated within 10 cm below the bedrock surface, where the flexural direction was opposite to the direction of thrust load. Due to the strong restriction of bedrock, the horizontal displacement of anchoring segment of the micropile was very small. Figure 6d is the schematic diagram of micropile deformation induced by soil movements, where the horizontal displacements of the loading segment were relatively large, and the flexural deformation occurred in the direction of soil movements, while the horizontal displacements of the anchoring segment were small and the flexural direction was opposite to the soil movements.

3.2.2 Deformation process

Figure 7 shows the pile-head horizontal displacement of micro-pipe pile group subjected to increasing thrust load at different row spacing. With increase of the lateral thrust, the deformation process of the micropile group could be divided into the following three stages by the developing characteristics of the horizontal displacement of pile head, as depicted in Fig. 8.

Stage I: Slow deformation stage. At this stage, the horizontal displacement of the pile head was less than 5 mm (as indicated in Figs.7 and 8), that is, no more than 1% of the loading depth (i.e., the pile length above the bedrock surface). The displacement was almost zero

at the beginning of the loading and then increased linearly and slowly with increase of the thrust load. The thrust load ranged from 0 to 3.5 kN during this stage when the row spacing of micropiles was 2D.

Stage II: Accelerating deformation stage. At this stage, the pile-head horizontal displacement ranged from 5 to 15 mm, corresponding to 1%–3% of the loading depth. The displacement displayed a nonlinear increasing trend with increase of the thrust load. The increasing rate of horizontal displacement was notably greater than that at Stage I. The loading range was relatively small during this stage, for example, it was approximately from 3.5 to 4.4 kN for the micropile group with 2D row spacing.

Stage III: Unstable deformation stage. At this stage, horizontal displacement of the pile head was larger than 15 mm, i.e., greater than 3% of the loading depth. The rate at which the horizontal displacement increased was significantly great that a small increase in thrust load could result in a large growth of the horizontal displacement of the pile head; this demonstrated that the micropile group had lost its anti-sliding capacity and entered the stage of instability. For the micro-pipe pile group at 2D row spacing, it would enter the unstable deformation stage when the thrust load increased to approximately 4.5 kN.

As shown in Figs. 7 and 8, although the micropile group lost its anti-sliding capacity when the horizontal displacement of pile head exceeded 3% of the loading depth, the deformation of micropile group could develop rapidly once the horizontal displacement of pile head was greater than 1% of the loading depth. This indicates that the anti-sliding structure may lose its bearing capacity in a short period after the pile-head displacement exceeds 1% of the loading depth. Therefore, from the designing point of view, the pile-head horizontal displacement should be controlled within 1% of the loading depth to ensure the safety margin to a certain extent. This standard is in accordance with the threshold of pile-head displacement required in the Code for Design of Retaining Engineering Structures of Railway Subgrade (Ministry of Railways 2006).

3.3 The critical thrust load of micropile group

From the forgoing analysis, it can be known that the composite structure would lose its anti-sliding capacity when the horizontal displacement of pile head was larger than 3% of the loading depth. Therefore, there would be a critical thrust load for failure, at which the horizontal displacement of pile head transformed from the accelerating deformation stage to the unstable deformation stage. To determine the critical thrust load of the micropile group, two linear equations were gained by linearly fitting the displacement-load curves of deformation stage II and III. The thrust load at the intersection of the two lines could be regarded as the critical thrust load, as shown in Fig. 8.

The critical thrust loads were calculated for micropile groups at row spacing of 2D, 4D, 6D and 8D, respectively. The results are tabulated in Table 2, from which it can be found that the anti-sliding capacity at row spacing of 6D was the largest, and that at row spacing of 2D was the smallest. The relative difference in critical load between the cases of row spacing of 6D and 2D reached up to approximately 24%, which implied that the row spacing of micropiles had an important influence on the anti-sliding capacity of micropile group.

Table 2 The critical thrust load of micropile group at different row spacing

Row spacing	2D	4D	6D	8D
The critical thrust load (kN)	4.61	5.38	5.70	5.35

Zeng and Xiao (2019) regarded the row spacing of micropiles had little effect on internal forces of micropile group based on the calculated results from a simplified method. However, it should be noted that in their calculations, some kinds of interactions between micropiles and the surrounding geomaterials, such as the pile group effects and the reinforcement of the surrounding soils, were not taken into consideration.

3.4 Bending moment of the micropile group

3.4.1 Bending moment distribution on micropiles

According to the theory of elastic beams, the relationship between the bending moment and the curvature of a pile is:

$$M = EI \cdot \varphi(y) = EI \cdot \frac{\varepsilon_1 - \varepsilon_2}{D} \tag{1}$$

where EI is the flexural rigidity of a pile; $\varphi(y)$ denotes the curvature of a pile expressed as follows:

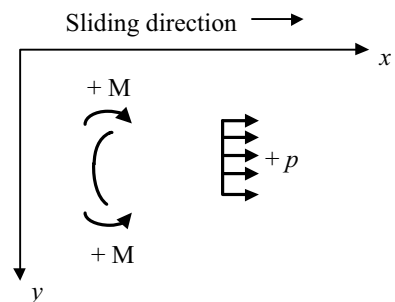
$$\varphi(y) = \frac{\varepsilon_1 - \varepsilon_2}{D} \tag{2}$$

where ε_1 and ε_2 are the longitudinal strains at the upslope side and downslope side of a pile at the same depth, respectively; D is the diameter of a pile; y is the distance between the strain gauge and the pile head.

According to Eq. (1), bending moment of the model pile at each measured point can be calculated from the test strain values of the pile, and the bending moment distribution curve of the pile can be obtained subsequently. The sign conventions for bending moment and earth pressure of the micropile are shown in Fig. 9.

Figure 10 depicts the bending moment distribution of each pile row in micropile group at row spacing of $6D$. The bending moment distribution of different pile rows was similar, which indicated the bending moments mainly located within the range of 10 cm above and below the bedrock surface. The directions of bending moment above and below the sliding zone were opposite, with the inflection point being about 3 cm above the bedrock surface, near top surface of the sliding zone. The maximum bending moment of the micropile occurred immediately below the bedrock surface. The distributed characteristics of bending moment along micropiles were consistent with that obtained by numerical simulations

Fig. 9 Sign conventions for bending moment (M) and earth pressure (p) of the micropile



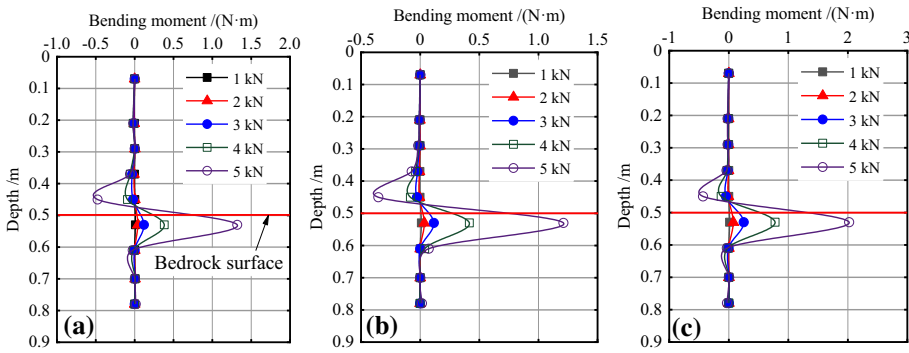


Fig. 10 Bending moment of micropile under various thrust load at row spacing of 6D. **a** The front pile row, **b** The middle pile row, **c** The rear pile row

on micropile groups retaining landslide (Li 2019). With the increase of thrust load, the rate at which the bending moment developed increased significantly in a nonlinear trend.

3.4.2 Bending moment evolution of the micropile group at row spacing of 2D

Figure 11 presents the comparison of bending moments of different pile rows in the micropile group at row spacing of 2D under various thrust loads, from which the coordinating ability of micropiles and geomaterials in the process of resisting lateral thrust load could be investigated. Figure 12 shows variation of the maximum bending moment of each pile row with the increased lateral thrust load.

From Figs.11 and 12, it can be found that for thrust load less than 3.5 kN, the bending moment value of the rear pile was almost the same as that of the middle pile; both of which were larger than that of the front pile row, indicating that the rear and middle rows of piles jointly resisted most of the thrust load at the initial stage of loading. As the thrust load increased, bending moments of different rows of micropiles tended to be the same, which indicated that the coordinating ability of micropiles and geomaterials among micropiles was better. The micropile group was just like a kind of conventional large cross-sectional anti-sliding pile to resist the lateral thrust load caused by soil movements. However, due to

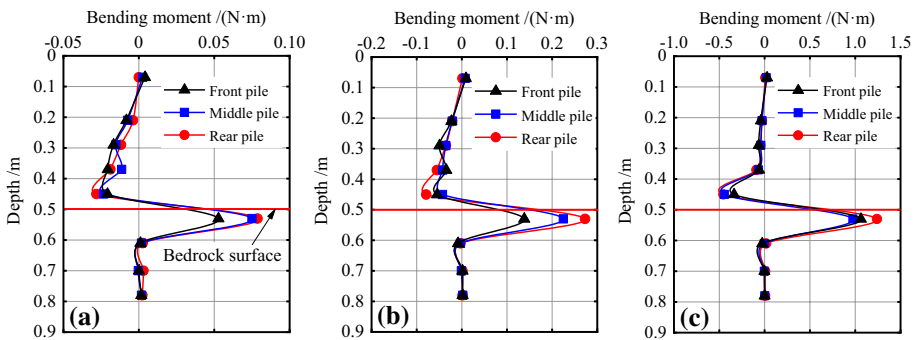
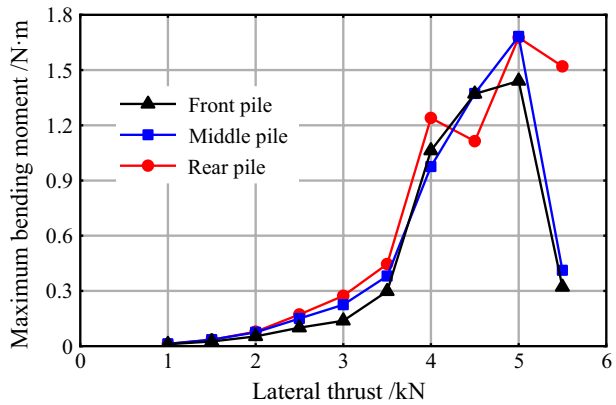


Fig. 11 Bending moment of micropiles at row spacing of 2D under the thrust loads of **a** 2.0 kN, **b** 3.0 kN and **c** 4.0 kN

Fig. 12 The maximum bending moment of micropiles versus thrust load (at row spacing of 2D)



the small row spacing of piles, the pile group effects were significant, which was detrimental to bearing capacity of the micropile group.

As shown in Fig. 12, when the lateral thrust load increased to 5 kN, all the bending moments of the piles reached a peak value; at this moment, the micropile group had entered the stage of unstable deformation according to the critical thrust load tabulated in Table 2. This illustrated that the micropile group had lost its effective resistance to the lateral thrust load. It is worth noting that the micropiles did not reach their ultimate structural bearing capacity, i.e., the micropiles themselves were not broken or pulled off, although the micropile group had lost the overall anti-sliding capacity. Therefore, besides the structural bearing capacity of the micropile group, the horizontal displacement of the pile-soil system should also be considered as an important indicator for the practical engineering design.

3.4.3 Bending moment evolution of the micropile group at row spacing of 6D

Figure 13 shows the bending moment comparison of different rows of micropiles for the case of 6D row spacing. For cases of lateral thrust load less than 5 kN, bending moment of the rear pile row was significantly larger than those of the middle and front pile rows that were basically the same, implying the greatest contribution of the rear pile row to the

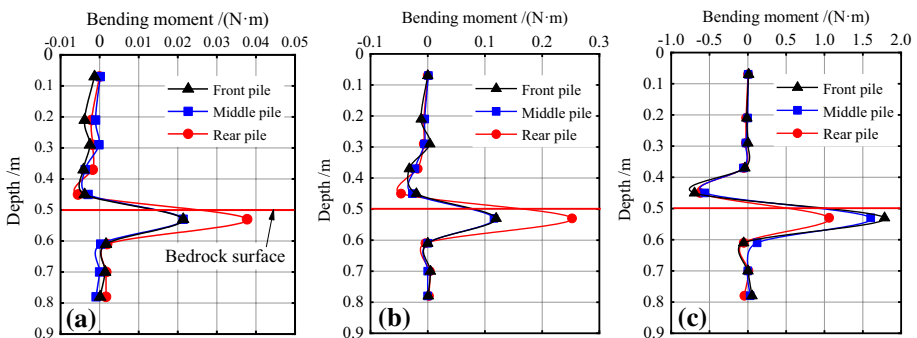


Fig. 13 Bending moment of micropiles at row spacing of 6D under the thrust loads of **a** 1.5 kN, **b** 3.0 kN and **c** 5.5 kN

overall anti-sliding capacity of the micropile group. Combining Figs. 13 and 14, it can be known that the bending moment of the rear pile row first reached a peak value at thrust load of 5 kN, and then dramatically decreased as the thrust load continued to increase, showing that the rear pile row had lost its anti-sliding ability. Subsequently, the bending moments of the other pile rows also began to rapidly decrease after reaching a peak value at thrust load of 5.5 kN, indicating that the micropile group had lost its overall anti-sliding bearing capacity due to the large deformations. This phenomenon indicated when the rear pile row lost its resisting ability, the micropile group was about to lose its overall anti-sliding bearing capacity immediately.

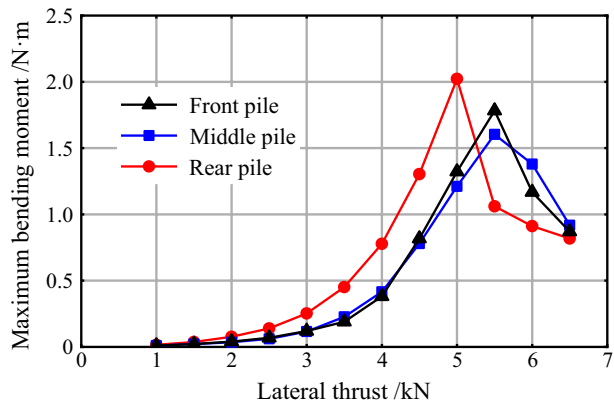
The characteristics of bending moment of micropile group at row spacing of 6D illustrated that with the increase of row spacing of micropiles, the integrated coordinating ability between micropiles and surrounding soils became smaller compared with the case of 2D row spacing. Nevertheless, the pile group effects on bearing capacity of micropile group had reduced, which led to an increase of anti-sliding capacity.

3.4.4 Bending moment evolution of the micropile group at row spacing of 8D

For row spacing of 8D, bending moments of micropiles under various lateral thrust loads were plotted in Fig. 15. When the lateral thrust load was small, for example, in the case of 1.5 kN thrust load, bending moments of the three pile rows were obviously different, where the rear pile row had the maximum bending moment, and the front row had the minimum one; this implied that as the row spacing of micropiles further increased after 6D, the integrated coordinating ability between micropiles and geomaterials would be further weakened.

Bending moments of the middle and front rows of piles tended to be the same and were significantly smaller than that of the rear pile row with the increased thrust load until the value of 5 kN, after which bending moment of the rear pile row decreased rapidly and was smaller than the other two pile rows, as shown in Fig. 15b, c and Fig. 16. The anti-sliding performance of the micropile group at row spacing of 8D was similar to that at row spacing of 6D, that is, bending moment of the rear pile row first reached a peak value and then decreased, immediately followed by the other two pile rows reaching a bending moment peak value at thrust load of 5.5 kN.

Fig. 14 The maximum bending moment of micropiles versus thrust load (at row spacing of 6D)



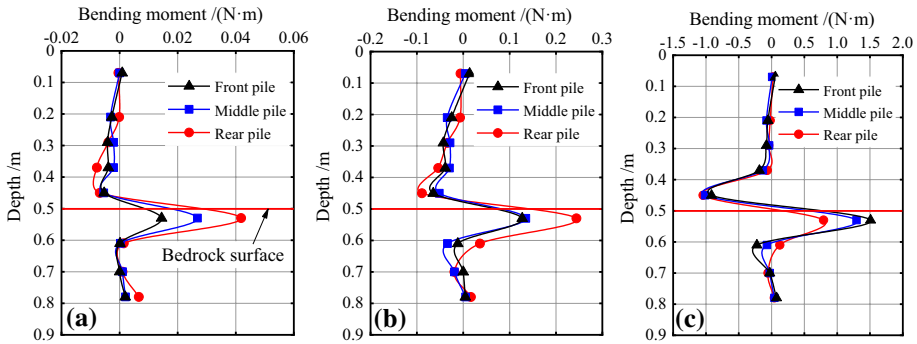
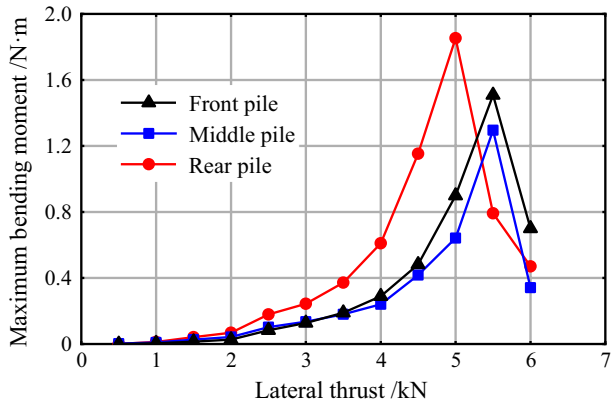


Fig. 15 Bending moment of micropiles at row spacing of 8D under the thrust loads of **a** 1.5 kN, **b** 3.0 kN and **c** 5.5 kN

Fig. 16 The maximum bending moment of micropiles versus thrust load (at row spacing of 8D)



3.5 Effects of micropile row spacing on anti-sliding capacity of micropile group

The soil among micropiles, which was restricted by micropiles and the roof plate, was an important part of the micropile group to resist the landslide thrust. Moreover, during the construction of micropile group, part of the grout would infiltrate into the surrounding soil under the grouting pressure, which not only improved the shear strength of the geomaterials around micropiles, but also improved the combination of micropiles and geomaterials. As a result, the interaction between micropiles, as well as the interaction between micropiles and the surrounding geomaterials, both played an important role in anti-sliding capacity of the micropile group.

As mentioned above, the row spacing of micropiles had an important effect on the anti-sliding capability of the composite micropile group. When the micropile row spacing was small, for example, in the case of row spacing of 2D, the grouted micro-pipe piles could effectively restrain the soil mass among piles to maintain a much better coordinating ability between micropiles, and micropiles and geomaterials. However, the volume of geomaterials surrounding micropiles that could be mobilized to resist the thrust load was small, and the pile group effects were relatively large, therefore, the overall anti-sliding capacity of micropile group was relatively small.

When the row spacing was large, for example, the row spacing of 8D in the tests, although the pile group effects reduced or even disappeared, and the volume of the soil among piles was larger, the overall coordinating ability between micropiles, as well as the coordinating ability between micropiles and surrounding soil both became smaller, due to the reduction of constraint of piles on geomaterials in vicinity. Therefore, a large row spacing of micropiles was not rational for mobilizing the anti-sliding capacity of micropile groups.

Thus, there would be an appropriate range of micropile row spacing at which the integrated anti-sliding capacity of micropile groups could be mobilized to a large extent, by reducing the disadvantageous influence of pile group effects, and meanwhile taking the advantage of coordinating ability between micropiles and the soil mass. In this study, for the case of 3×3 configuration of grouted micro-pipe pile groups, the anti-sliding capacity was largest at row spacing of 6D, followed by row spacing of 4D and 8D. The anti-sliding capacity was smallest for row spacing of 2D. These results demonstrate that when the row spacing of micropiles ranges from 4 to 8D, the 3×3 micropile groups have a much better coordinating ability and the pile group effects is relatively small; the micropiles and surrounding soils can work together effectively to resist the landslide thrust. For practical engineering application, the longitudinal row spacing of micropiles is recommended to be 4–8 times of the micropile diameter.

4 Conclusions

Through experiments on the 3×3 grouted micro-pipe pile groups anchored in bedrock subject to lateral soil movements, the active earth pressure distribution, bending moment characteristics, deformation process, and especially the effects of row spacing on anti-sliding performance of micropile groups were investigated. The main conclusions are as follows.

- (1) The micropiles and the geomaterials surrounding micropiles work in tandem to stabilize the landslide. The row spacing of micropiles in line significantly affects the anti-sliding bearing capacity of the micropile group, by affecting the interaction between micropiles, as well as the interaction between micropiles and geomaterials. The row spacing of 4–8 times the micropile diameter is recommended for practical landslide-stabilization engineering.
- (2) The deformation process of the micropile group can be divided into three stages: (i) Slow deformation stage where the pile-head displacement is less than 1% of the loading depth. (ii) Accelerating deformation stage where the pile-head displacement increases from 1% to 3% of the loading depth. (iii) Unstable deformation stage where the pile-head displacement exceeds 3% of the loading depth. For design of practical slope-stabilization engineering, it is recommended that the horizontal displacement of pile head should be controlled within 1% of the loading depth.
- (3) The active earth pressure on micropiles distributes triangularly. The earth thrust on the rear pile row is the largest and that on the front pile row is the smallest. As the thrust load increases, much more thrust load transfers to the middle and front pile rows; this may result in the active earth pressure ratios of the rear, middle and front pile rows up to 1:0.60:0.44.
- (4) The flexural directions of micropiles above and below the sliding zone are opposite, with the maximum bending moment close to the bedrock surface in the anchoring

segment. As the thrust load increases, the bending moment of the rear pile row first reaches a peak value, and then greatly decreases; this phenomenon indicates that the micropile group is going to lose its anti-sliding ability.

Funding This research was supported by the National Natural Science Foundation of China (Grant No. 40702044).

Declarations

Conflict of interest The authors declare no conflicts of interest.

References

- Aboutabikh M, Soliman AM, El Naggar MH (2020) Performance of hollow bar micropiles using green grout incorporating treated oil sand waste. *J Build Eng* 27:100964. <https://doi.org/10.1016/j.jobbe.2019.100964>
- Bruce DA, Juran I (1997) Drilled and grouted micropiles: state-of-practice review, volume II: design, vol no FHWA-RD-96-017. United States Department of Transportation, USA
- Bruce DA, Cadden AW, Sabatini PJ (2005) Practical advice for foundation design-micropiles for structural support. *GSP 131 Contemporary Issues in Foundation Engineering*. [https://doi.org/10.1061/40777\(156\)14](https://doi.org/10.1061/40777(156)14)
- Cantoni R, Collotta T, Ghionna V (1989) A design method for reticulated micropile structures in sliding slopes. *Ground Eng* 22(4):41–47. [https://doi.org/10.1016/0148-9062\(89\)91811-1](https://doi.org/10.1016/0148-9062(89)91811-1)
- Chandrasekaran SS, Sayed Owaise R, Ashwin S et al (2013) Investigation on infrastructural damages by rainfall-induced landslides during November 2009 in Nilgiris, India. *Nat Hazards* 65:1535–1557. <https://doi.org/10.1007/s11069-012-0432-x>
- Froude MJ, Petley DN (2018) Global fatal landslides occurrence from 2004 to 2016. *Nat Hazard* 18(8):2161–2181. <https://doi.org/10.5194/nhess-18-2161-2018>
- Ghosh P, Pandey SK, Rajesh S (2021) Seismic stability of slopes reinforced with micropiles—a numerical study. In: Sitharam T, Jakka R, Kolathayar S (eds) Latest developments in geotechnical earthquake engineering and soil dynamics Springer transactions in civil and environmental engineering. Springer, Singapore. https://doi.org/10.1007/978-981-16-1468-2_18
- Gupta RK, Chawla S (2020) Finite element analysis of micropile reinforced subgrade in railway tracks. In: Latha Gali M, Rao PR (eds) Geotechnical characterization and modelling. Lecture notes in civil engineering, vol 85. Springer, Singapore. https://doi.org/10.1007/978-981-15-6086-6_60
- Hu TF, Liu JK, Zhu BZ, Zheng J (2016) Study on sliding characteristics and controlling measures of colluvial landslides in Qinghai-Tibet Plateau. *Proced Eng* 143:1477–1484. <https://doi.org/10.1016/j.proeng.2016.06.174>
- Iai S (1989) Similitude for shaking table test on soil-structure-fluid model in 1-g gravitational field. *Soils Found* 29(1):105–118. <https://doi.org/10.3208/sandf1972.29.105>
- Juran I, Benslimane A, Bruce DA (1996) Slope stabilization by micropile reinforcement. *Landslides* 5:1715–1726
- Kim D, Kim G, Kim I, Lee J (2018) Assessment of load sharing behavior for micropiled rafts installed with inclined condition. *Eng Struct* 172:780–788. <https://doi.org/10.1016/j.engstruct.2018.06.058>
- Kumar JS, Nusari MS, Purushotam D et al (2021) Effectiveness of geocell wall, geogrid and micropile anchors for mitigation of unstable slopes. *Geoenviron Disasters* 8:11. <https://doi.org/10.1186/s40677-021-00185-z>
- Li N, Men Y, Yuan L et al (2020) Study on the mechanical characteristic of micropiles supporting landslide under step-loadings. *Geotech Geol Eng* 38:2761–2771. <https://doi.org/10.1007/s10706-020-01184-x>
- Li J (2019) Study on interaction mechanism between micro-piles and landslides and soil-arch effect. Dissertation, Chang'an University (In Chinese)
- Liu Z, Yan Z, Wang X, Li J, Qiu Z (2021) Effect of the inclined pile-soil arch in a soil landslide reinforced with anti-sliding piles. *Nat Hazards* 106:2227–2249. <https://doi.org/10.1007/s11069-021-04541-y>

- Loehr JE, Bowders JJ, Owen JW (2000) Slope stabilization with recycled plastic pins. *J Transp Res Record* 1714(1):1–8. <https://doi.org/10.3141/1714-01>
- Ministry of Railways (2006) Code for design of retaining engineering structures of railway subgrade (TB10025-2006). China Railway Publishing House, Beijing (**In Chinese**)
- Prat Pere C (2017) Numerical investigation into the failure of a micropile retaining wall. *Comput Geotech* 81:262–273. <https://doi.org/10.1016/j.compgeo.2016.08.026>
- Sun SW, Zhu BZ, Wang JC (2013) Design method for stabilization of earth slopes with micropiles. *Soils Found* 53(4):487–497. <https://doi.org/10.1016/j.sandf.2013.06.002>
- White DJ, Thompson MJ, Suleiman MT, Schaefer VR (2008) Behavior of slender piles subject to free-field lateral soil movement. *J Geotech Geoenviron Eng* 134(4):428–436. [https://doi.org/10.1061/\(ASCE\)1090-0241\(2008\)134:4\(428\)](https://doi.org/10.1061/(ASCE)1090-0241(2008)134:4(428))
- Xiang B, Zhang LM, Zhou LR, He YY, Zhu L (2015) Field lateral load tests on slope-stabilization grouted pipe pile groups. *J Geotech Geoenviron Eng* 141(4):04014124. [https://doi.org/10.1061/\(ASCE\)GT.1943-5606.0001220](https://doi.org/10.1061/(ASCE)GT.1943-5606.0001220)
- Xiao SG, Cui K, Zhou DP, Feng J (2009) Analysis of a new combined micropile structure for preventing slope slippage and its application in a practical project. *ICCTP 2009, ASCE* 1–11. [https://doi.org/10.1061/41064\(358\)5](https://doi.org/10.1061/41064(358)5)
- Yang B, Zhou Z, Hou J, Yang T, Zhang J (2022) Failure characteristics and mechanism of deposit slopes with bedrock for different soil moisture contents under seismic load. *Soil Dyn Earthq Eng* 154:107128. <https://doi.org/10.1016/j.soildyn.2021.107128>
- Zeng JX, Xiao SG (2019) A simplified analytical method for stabilizing micropile groups in slope engineering. *Int J Civ Eng* 18:199–214. <https://doi.org/10.1007/s40999-019-00436-z>
- Zhang F, Peng J, Huang X et al (2021) Hazard assessment and mitigation of non-seismically fatal landslides in China. *Nat Hazards* 106:785–804. <https://doi.org/10.1007/s11069-020-04491-x>

Publisher's Note Springer Nature remains neutral with regard to jurisdictional claims in published maps and institutional affiliations.